Production of the ΞN dibaryon as a weakly bound system in *pp* collisions

Tian-Chen Wu,[1] Atsushi Hosaka,[2,3,*] and Li-Sheng Geng[1,4,5,6,†]

[1]*School of Physics, Beihang University, Beijing 102206, China*
[2]*Research Center for Nuclear Physics (RCNP), Ibaraki, Osaka 567-0047, Japan*
[3]*Advanced Science Research Center, Japan Atomic Energy Agency, Tokai, Ibaraki 319-1195, Japan*
[4]*Peng Huanwu Collaborative Center for Research and Education, Beihang University, Beijing 100191, China*
[5]*Beijing Key Laboratory of Advanced Nuclear Materials and Physics, Beihang University, Beijing 102206, China*
[6]*Southern Center for Nuclear-Science Theory (SCNT), Institute of Modern Physics, Chinese Academy of Sciences, Huizhou 516000, China*

(Received 12 November 2023; accepted 2 May 2024; published 7 June 2024)

The ΞN interaction plays an important role in understanding the long-anticipated *H* dibaryon. Recent lattice QCD calculations verified the attractive nature of the ΞN interaction. On the other hand, whether it is strong enough to generate a bound state remains inconclusive. In this work, assuming it can generate a weakly bound state, we study the yields of the ΞN dibaryon for different binding energies in *pp* collisions at 7 TeV using the coalescence model and the transport model PACIAE. The yields are estimated first numerically and then analytically, adopting a Yukawa-type wave function. In particular, we find that in the weak binding limit, there exists a universal relation between the yield and the binding energy, valid for *pp* collisions.

DOI: 10.1103/PhysRevD.109.114009

I. INTRODUCTION

In the KEK-E373 experiment, the first clear evidence of a deeply bound state of Ξ baryon and nitrogen-14 nucleus was found [1]. However, there is no direct experimental evidence for the existence of the ΞN dibaryon so far [2–6]. Studying the simplest ΞN dibaryon (often referred to as the *H* dibaryon [7]) plays a fundamental role in understanding the nonperturbative strong force in a more complex system, such as the bound state of Ξ baryon and nitrogen-14 nucleus. Recent lattice QCD simulations [8] and correlation function studies [9] indicate an attractive ΞN interaction. With the ΞN potential from the latest lattice QCD simulation [8], Hiyama *et al.* found that the ΞN system cannot bind [10], consistent with the studies performed in chiral effective field theories [9,11]. On the other hand, with the ESC08c potential, the ΞN system can develop a shallow bound state with a binding energy of a few MeV [10,12,13]. Under such an unsettled situation, in this work, we would like to propose an alternative way by studying the production process of the ΞN dibaryon in *pp* collisions.

The coalescence model is a well-established method to describe the production processes of composite particles. To apply the coalescence model to the ΞN dibaryon, we need two essential inputs. One is to find a proper process to produce the constituent particles Ξ and *N*. Since the yields of Ξ and *N* are well studied in LHC experiments, e.g., inelastic proton-proton (*pp*) collisions [14–16], it is reasonable to choose the *pp* collisions for this purpose. In our work, this process is simulated by the transport model PACIAE [17]. The other essential part is correctly setting conditions to constrain the constituent particles in phase space. The simplest condition is the cutoff condition [18,19], where the constituent particles combine when their relative distance and relative momentum are smaller than a specified cutoff. Another microscopic approach is the Wigner density approach [18,20–26], which relies on the wave function of the composite particle.

If Ξ and *N* can bind, it will likely be a shallow bound state. If the ΞN dibaryon is a resonance, it is probably a Feshbach resonance, whose seed is a ΞN bound state coupled with the open channel of ΛΛ. We can reasonably assume that the shape of the wave function of the ΞN resonance is similar to that of the ΞN bound state. Therefore, our work assumes the ΞN dibaryon as a weakly bound state. The wave function of the ΞN dibaryon at large distances should behave as the Yukawa function for a short-range

*hosaka@rcnp.osaka-u.ac.jp
†lisheng.geng@buaa.edu.cn

potential. The range of the wave function is only related to the reduced mass and the binding energy E_B of the bound state. This means that the yield of ΞN depends primarily on the binding energy E_B, a universal phenomenon, as we will demonstrate in this work.

This article is organized as follows. In Sec. II, we briefly introduce the transport model PACIAE and the coalescence model adopting the Yukawa-type wave function. The formalism is presented in both numerical and analytical ways. In Sec. III, we discuss the numerical and analytical results then the universal phenomenon. Finally, we present a summary in Sec. IV.

II. FORMALISM

The production of a composite particle is naturally divided into two steps: the production of constituent hadrons and their combination into the composite particle. We employ the transport model PACIAE [17] for the former step, and the coalescence model with the Wigner function approach for the latter step.

A. PACIAE model

The PACIAE model is a transport model based on the event generator PYTHIA [27]. It describes high-energy collisions, such as e^+e^- collisions, hadron-hadron collisions, and nucleus-nucleus collisions. Similar to the PYTHIA model, the PACIAE model also simulates the collision process in terms of parton initiation and hadronization, but with additional transport processes [17]. In parton initiation, hadron-hadron collisions are decomposed into parton-parton interactions. The hard part is treated by the leading order perturbative QCD, while the soft part involves some phenomenological modeling. Hadronization and decay are then expected after the parton initiation. The most significant difference between the transport model PACIAE and the generator PYTHIA is that the former introduces the transport processes, considering that the thermodynamical interactions cannot be neglected in the multiparticle states.

The tunable parameters in the PACIAE model are those that determine the probabilities of different quark pairs created from the vacuum or in the hadronization functions. The PYTHIA Perugia 2011 (P2011) cannot well simulate the experimental yields of Ξ and Ω, where the yield of Ω is several times smaller than the experimental measurement [15]. This shows the insufficiency of this simulation mode in describing the production of strange quarks. Moreover, the structure of Nambu-Goldstone bosons is more complicated than the one encoded in the Lund string model. Since in our simulation we are more interested in the productions of baryons, especially multistrange baryons, we tuned the parameters so that the simulation results are in better agreement with the experimental yields of N, Ξ, and Ω, and ignore the discrepancy in the yields of mesons.

B. Coalescence model

The basic idea of the coalescence model is that the constituent particles of a shallow-bound composite particle, whose binding energy is small compared to the evolution temperature, are difficult to combine until the whole system reaches the kinetic freeze-out. This implies the final state approximation [20], where "final state" indicates that the constituent particles experience almost no interaction with other hadrons. The contribution from intermediate interactions before kinetic freeze-out to the yield of the composite particle can be neglected. In addition, the coalescence time is short compared to the interaction time in the final state. Therefore, the coalescence process can be described in a sudden approximation [18]. As a result, we can interpret the formation of a composite particle as a trace over the density of the source $\hat{\rho}_S$ in the final state, which is the phase space distribution of constituent particles, and the density of the composite particle $\hat{\rho}_C = |\Psi_C\rangle\langle\Psi_C|$, i.e., $\mathrm{tr}[\hat{\rho}_S\hat{\rho}_C] = \mathrm{tr}[\hat{\rho}_S|\Psi_C\rangle\langle\Psi_C|]$ [18].

It is important to note that the density of the source is described by a semiclassical transport model, while the wave function of the composite particle is from quantum theory. Thus, transformation is needed to combine these two models. For this, the Wigner transform is an effective method. In this approach, both the density of the source $\hat{\rho}_S$ and the density of the composite particle $\hat{\rho}_C$ are transformed to Wigner densities $\hat{\rho}_S^W$ and $\hat{\rho}_C^W$.

The n-body Wigner density of the source calculated from the transport model can be written as [18]

$$\hat{\rho}_S^W(\boldsymbol{x}_1,\boldsymbol{p}_1,\ldots,\boldsymbol{x}_n,\boldsymbol{p}_n) = \left\langle \sum_{(c)} \prod_{i=1}^{n} (2\pi)^3 \delta^3(\boldsymbol{x}_i - \tilde{\boldsymbol{x}}_i)\delta^3(\boldsymbol{p}_i - \tilde{\boldsymbol{p}}_i) \right\rangle, \quad (1)$$

where (c) is the index of combinations in a collision event, i is the index of hadrons in each combination, $\tilde{\boldsymbol{x}}_i$ and $\tilde{\boldsymbol{p}}_i$ are the phase space coordinates of particle i in the PACIAE final state, and $\langle\ldots\rangle$ denotes that the result is averaged over all the event runs. The Wigner density of the composite particle can be obtained by the Wigner transform,

$$\hat{\rho}_C^W(\boldsymbol{r}_1,\boldsymbol{q}_1,\ldots,\boldsymbol{r}_{n-1},\boldsymbol{q}_{n-1}) = \int \Psi_C^*\left(\boldsymbol{r}_1 + \frac{1}{2}\boldsymbol{y}_1,\ldots,\boldsymbol{r}_{n-1} + \frac{1}{2}\boldsymbol{y}_{n-1}\right)\Psi_C\left(\boldsymbol{r}_1 - \frac{1}{2}\boldsymbol{y}_1,\ldots,\boldsymbol{r}_{n-1} - \frac{1}{2}\boldsymbol{y}_{n-1}\right) \times e^{-i\boldsymbol{q}_1\cdot\boldsymbol{y}_1}\cdots e^{-i\boldsymbol{q}_{n-1}\cdot\boldsymbol{y}_{n-1}} d\boldsymbol{y}_1\cdots d\boldsymbol{y}_{n-1}, \quad (2)$$

where $\boldsymbol{r}_{n-1}$ and $\boldsymbol{q}_{n-1}$ are the $n-1$ relative coordinates corresponding to the position and momentum coordinates $\boldsymbol{x}_n$ and $\boldsymbol{p}_n$. Then, the differential and total yield Y from an n-body system averaged in each event is [18,28]

$$\frac{dY}{d\boldsymbol{P}} = g\int \hat{\rho}_S^W(\boldsymbol{x}_1,\boldsymbol{p}_1,\ldots,\boldsymbol{x}_n,\boldsymbol{p}_n)\hat{\rho}_C^W(\boldsymbol{r}_1,\boldsymbol{q}_1,\ldots,\boldsymbol{r}_{n-1},\boldsymbol{q}_{n-1})\delta^3(\boldsymbol{P}-(\boldsymbol{p}_1+\cdots\boldsymbol{p}_n))\frac{d\boldsymbol{x}_1 d\boldsymbol{p}_1}{(2\pi)^3}\cdots\frac{d\boldsymbol{x}_n d\boldsymbol{p}_n}{(2\pi)^3},$$
$$Y = g\left\langle \sum_{(c)} \hat{\rho}_C^W(\tilde{\boldsymbol{r}}_1,\tilde{\boldsymbol{q}}_1,\ldots,\tilde{\boldsymbol{r}}_{n-1},\tilde{\boldsymbol{q}}_{n-1})\right\rangle, \tag{3}$$

where $\boldsymbol{P}$ is the total momentum of the composite particle, $\tilde{\boldsymbol{r}}_{n-1}$ and $\tilde{\boldsymbol{q}}_{n-1}$ are the relative position and momentum coordinates calculated with the position coordinate $\tilde{\boldsymbol{x}}_n$ and the momentum coordinate $\tilde{\boldsymbol{p}}_n$ of the primary hadrons in each combination (c) from the transport model. The additional factor g is the spin statistical factor, which is $1/4$ in our work.

C. Use of the Yukawa function

In Ref. [8], lattice QCD simulations found that the ΞN interaction is much stronger than the $\Lambda\Lambda$ and the $\Xi N-\Lambda\Lambda$ interactions. As a result, it is impossible to form a $\Lambda\Lambda$ bound state. On the other hand, the ΞN interaction can barely form a bound state, though the current lattice QCD potential extracted from Ref. [8] cannot, as shown in Ref. [10]. We learned from a private communication from the HAL QCD collaboration that lattice QCD simulations are ongoing at the physical point and with higher statistics. They will tell whether the ΞN interaction is sufficient or not to support a bound state. We note that the rather weak $\Lambda\Lambda$ and $\Lambda\Lambda-\Xi N$ interactions compared to the ΞN interaction means that although coupled-channel dynamics tells that the ΞN bound state has a $\Lambda\Lambda$ component, the contribution of the $\Lambda\Lambda$ component to the formation of the ΞN bound state can be safely neglected.

The potential takes a general Yukawa form for the ΞN dibaryon [8], which vanishes sufficiently fast at large distances. Therefore, the wave function can be approximated as the Yukawa function at large distances. However, the Yukawa function has a singular point at the origin. This can be avoided by introducing a form factor $\Lambda^2/(q^2+\Lambda^2)$, which characterizes the size of hadrons. We set the cutoff Λ at 0.8 GeV corresponding to a size of $\langle r^2\rangle^{1/2}\sim 0.6$ fm. The wave function then has the following form:

$$\Psi_C(r) = A\left(\frac{e^{-\beta r}}{r}-\frac{e^{-\Lambda r}}{r}\right), \tag{4}$$

where $\beta=\sqrt{2\mu E_B}$, μ is the reduced mass, E_B is the binding energy, and A is the normalization constant $A=\sqrt{\beta\Lambda(\beta+\Lambda)/(2\pi(\beta-\Lambda)^2)}$.

Since the analytical form of the Wigner density corresponding to the wave function in Eq. (4) is hard to obtain, we numerically expand the wave function in terms of the Gaussian bases,

$$\Psi_C(r) = \sum_{i=1}^{N} c_i\left(\frac{2\omega_i}{\pi}\right)^{3/4} e^{-\omega_i r^2}, \tag{5}$$

where $N=50$ is the number of bases, ω_i characterizes the width of the Gaussian bases, and c_i is the corresponding weighting factor. With this expansion, the Wigner density has the form

$$\begin{aligned}\hat{\rho}_C^W(\boldsymbol{r},\boldsymbol{q}) = {}& 8\sum_{i=1}^{N} c_i^2 \exp\left(-2\omega_i r^2-\frac{q^2}{2\omega_i}\right)\\ &+16\sum_{i>j}^{N} c_i c_j\left(\frac{4\omega_i\omega_j}{(\omega_i+\omega_j)^2}\right)^{3/4}\exp\left(-\frac{4\omega_i\omega_j}{\omega_i+\omega_j}r^2\right)\\ &\times\exp\left(-\frac{q^2}{\omega_i+\omega_j}\right)\cos\left(2\frac{\omega_i-\omega_j}{\omega_i+\omega_j}\boldsymbol{r}\cdot\boldsymbol{q}\right).\end{aligned} \tag{6}$$

Then it is convenient to calculate the yield of ΞN numerically, but it is not transparent to show the connection between the yield Y and the binding energy E_B. To better understand the relation, we need to make some approximations when we insert Eq. (4) into Eq. (2). According to the mean value theorem, $\hat{\rho_C}^W(\tilde{\boldsymbol{r}},\tilde{\boldsymbol{q}})$ in Eq. (3) for a binding energy E_B in one combination (c) for Ξ and N is

$$\hat{\rho}_C^W(\tilde{\boldsymbol{r}},\tilde{\boldsymbol{q}}) \sim C_1 A^2(e^{-\beta C_2}-e^{-\Lambda C_2})\left(\frac{1}{\beta+C_3}-\frac{1}{\Lambda+C_3}\right), \tag{7}$$

where C_1, C_2, and C_3 are functions of $\tilde{\boldsymbol{r}}$ and $\tilde{\boldsymbol{q}}$. For the ΞN dibaryon, the binding energy E_B is small, so $A\sim\sqrt{\beta}$ when $E_B\to 0$. For the same reason, $\frac{1}{\beta+C_3}\sim\frac{1}{C_3}$ and $e^{-\beta C_2}-e^{-\Lambda C_2}\sim e^{-\beta C_2}$. In this weak binding limit, one has

$$\hat{\rho}_C^W(\tilde{\boldsymbol{r}},\tilde{\boldsymbol{q}}) \sim C_1\beta e^{-\beta C_2}\left(\frac{1}{C_3}-\frac{1}{\Lambda+C_3}\right) \equiv C'\beta e^{-\beta C_2}. \tag{8}$$

The total yield is the summation of all the combinations. For each combination(c) we have $C'^{(c)}$ and $C_2^{(c)}$, thus the total yield Y is

$$Y = g\left\langle \sum_{(c)} \hat{\rho}_C^W(\tilde{\boldsymbol{r}}, \tilde{\boldsymbol{q}}) \right\rangle \sim g\beta \left\langle \sum_{(c)} C'^{(c)} e^{-\beta C_2^{(c)}} \right\rangle. \quad (9)$$

Inspired by the form of Wigner densities of the Yukawa function and converting the sum into an integral, we assume an approximation for Eq. (9) as follows:

$$Y \sim g\beta(\xi_1 e^{-\beta\xi_2} + P(\beta)) \sim g\sqrt{2\mu E_B}\xi_1 e^{-\sqrt{2\mu E_B}\xi_2}, \quad (10)$$

where the parameters ξ_1 and ξ_2 can be determined by fitting to the simulation data, and $P(\beta)$ is a polynomial serving as a correction term. In Sec. III B, the polynomial is taken to be a constant, $P(\beta) = \xi_3$. In the case of a small binding energy, the yield then has the following asymptotic form:

$$Y \sim \sqrt{E_B} \sim \frac{1}{R}, \quad (11)$$

where $R \approx 1/(2\sqrt{\mu E_B})$ [29] is the root-mean-square radius of the ΞN dibaryon. We will fit this formula to the simulation data in Sec. III B to verify the approximation.

III. RESULTS AND DISCUSSIONS

A. Productions of normal hadrons

First, let us obtain the yields of ordinary hadrons in the PACIAE simulation. As mentioned in Sec. II A, we focus on the productions of baryons, especially strange baryons, so we have mainly tuned the parameters related to the s quark. We kept all the parameters at their default values, except for PARJ(1) = 0.06, PARJ (2) = 0.44, and PARJ(3) = 0.8, where PARJ(1) (Default = 0.10) is for the suppression of diquark-antidiquark pair production compared with quark-antiquark production, PARJ(2) (Default = 0.30) for the suppression of s quark pair production with u or d pair production, and PARJ(3) (Default = 0.4) for the extra suppression of strange diquark production compared with the normal suppression of strange quarks [27]. The so-obtained simulation results for the total yields of baryons are shown in Table I, and the p_T distributions of the yields of Ξ and Ω are shown in Figs. 1 and 2. We find that the simulation results agree with the experimental data. (The data are selected in the rapidity region $|y| < 0.5$, and therefore, they are missing in the small transverse momentum region.)

TABLE I. Experimental and simulated yields of primary hadrons at $|y| < 0.5$ per pp collision event at $\sqrt{s} = 7$ TeV.

Particle	Data [15,16]	Simulation (tuned)	Simulation (default)
$\Xi^-(\times 10^{-3})$	$8.0 \pm 0.1^{+0.7}_{-0.5}$	7.93	3.78
$\Xi^+(\times 10^{-3})$	$7.8 \pm 0.1^{+0.7}_{-0.5}$	8.06	3.72
$\Omega^-(\times 10^{-3})$	$0.67 \pm 0.03^{+0.08}_{-0.07}$	0.684	0.120
$\Omega^+(\times 10^{-3})$	$0.68 \pm 0.03^{+0.08}_{-0.06}$	0.728	0.106
p	0.124 ± 0.009	0.132	0.210
$\overline{p}$	0.123 ± 0.010	0.131	0.208

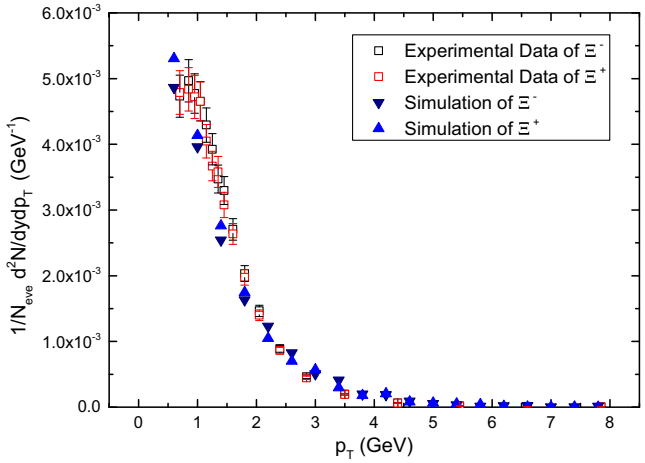

FIG. 1. p_T distribution of the yield of Ξ at $|y| < 0.5$ in bins of 0.4 GeV, where the squares are the experimental data from ALICE [15] and the triangles are the simulation results.

B. Yield of ΞN dibaryon

With the Wigner density approach, we numerically obtain the yields of the ΞN dibaryon for different binding energies according to Eq. (6), which are shown in Table II and Fig. 3. The production yields are of the order of 10^{-4}, somewhat smaller than those of Ω by 1 order of magnitude. However, we expect that the ΞN dibaryon can be found if it has a binding energy of a few MeV. Although there is no direct experimental evidence for the ΞN dibaryon so far, we can search for its signature using femtoscopic techniques [2,3], and also K induced reactions [4,30]. To estimate the impact of parameter tuning, we use the default parameters

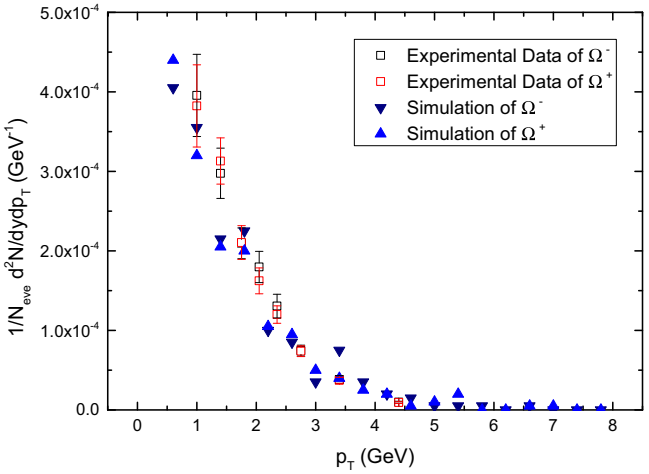

FIG. 2. p_T distribution of the yield of Ω at $|y| < 0.5$ in bins of 0.4 GeV, where the squares are the experimental data from ALICE [15] and the triangles are the simulation results.

TABLE II. Averaged yield of ΞN dibaryon in pp collisions at $\sqrt{s} = 7$ TeV obtained from the Wigner function approach per pp event, containing charge conjugated states. The binding energy $E_B = 1.655$ MeV is predicted by the ESC08c potential [12].

Binding energy E_B (MeV)	0.10	0.50	1.00	1.66	3.50	5.00	7.50	10.00	12.50
Ξp ($\times 10^{-4}$)	0.12	0.23	0.30	0.36	0.45	0.49	0.53	0.55	0.57
Ξn ($\times 10^{-4}$)	0.13	0.25	0.32	0.38	0.47	0.51	0.56	0.59	0.60
Total ($\times 10^{-4}$)	0.24	0.48	0.62	0.74	0.92	1.00	1.08	1.14	1.17

of the PACIAE, and find the yield is about 75% of those obtained with the tuned parameters; the yield of Ξ with the default parameters is about 45% and that of N is about 170% of those obtained with the tuned values, as shown in Table I. The yields tend to approach zero as $E_B \to 0$. This is expected because when the binding energy is small, the wave function extends far away, which leads to a vanishing constant A, and therefore, the yield goes to zero.

Now we fit the simulation results with the formula of Eq. (10). The fitted parameters are listed in Table III. We have three sets of parameters for the three lines since ξ_1, ξ_2, and ξ_3 are related to the properties of different sources depending on the configurations. As shown in Fig. 3, the fits reproduce the simulation data very well with the $\sqrt{E_B}$ dependence for small E_B. This is a universal phenomenon when the production region is relatively small as in pp collisions, which was referred to as short-distance production in Refs. [31–33]. We discuss this behavior later using the Wigner densities as shown in Figs. 5 and 6.

We can also interpret the trend in terms of the root-mean-square radius of the system. As shown in Fig. 4, the yield of ΞN is smaller when it has a larger size. This behavior seems contradictory to the one drawn in Refs. [21,34], which claimed that the yield would be more significant if the hadronic molecule was more loosely bound. To understand this apparent discrepancy, recall that the yield reflects the overlap of the Wigner density of the source and the composite particle. The Wigner density of the composite particle will extend in the position space and shrink in the momentum space as the size of the composite particle grows, as shown in Fig. 5. However, we note that the Wigner density of the source differs significantly between pp collisions and heavy-ion collisions, as shown in Fig. 6. In the final state of relativistic heavy-ion collisions, the spatial part is uniformly distributed in phase space since the volume of QGP is very large compared with the size of the composite particle [21,34], as the brightest band in Fig. 6(b) shows. On the contrary, in the final state of pp collisions, the hadrons are produced mainly in the area $r < 4$ fm, centering around 2 fm, as the brightest part in Fig. 6(a) shows. Intuitively, one expects that in pp collisions, the overlap will get smaller

TABLE III. Fitted parameters for the yields of the ΞN dibaryon.

Parameter	ξ_1 (fm $\times 10^{-3}$)	ξ_2 (fm)	ξ_3 (fm $\times 10^{-3}$)
$\Xi^- p$	0.7957	2.3072	0.1828
$\Xi^0 n$	0.8411	2.3531	0.1997
Total	1.6367	2.3308	0.3826

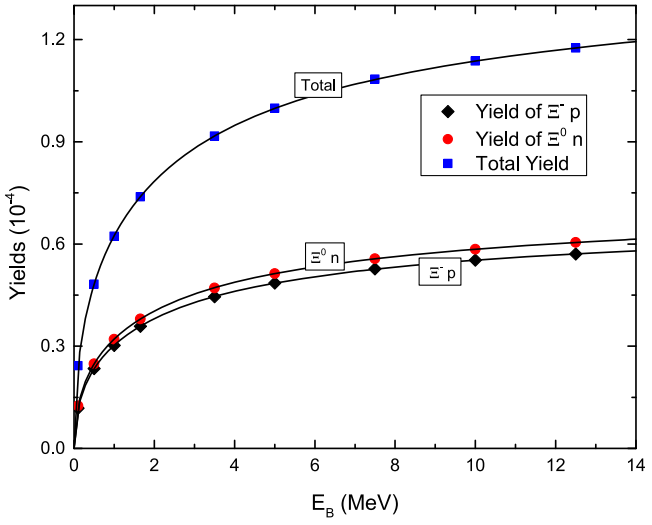

FIG. 3. Yields of the ΞN dibaryon for different binding energies E_B, where the solid diamonds/squares/circles are simulation data, and the lines are the analytic results fitted to the simulation data.

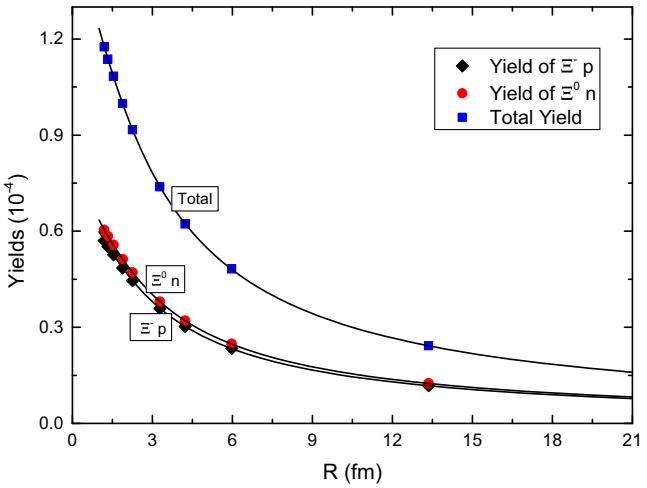

FIG. 4. Yields of the ΞN dibaryon for different root-mean-square radii R, where the solid diamonds/squares/circles are simulation data, and the lines are analytic results fitted to the simulation data.

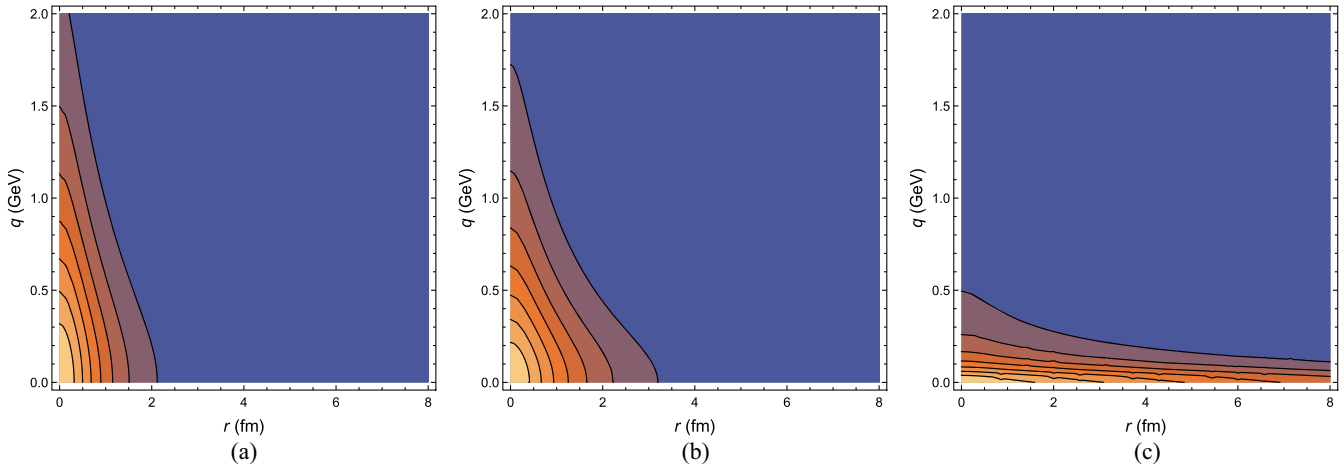

FIG. 5. The Wigner densities (with the angle between $\boldsymbol{r}$ and $\boldsymbol{q}$ is $\pi/2$) of the ΞN dibaryon for different binding energies and sizes, where parts (a), (b), and (c) correspond to $E_B = 12.5$, 5, and 0.1 MeV, respectively.

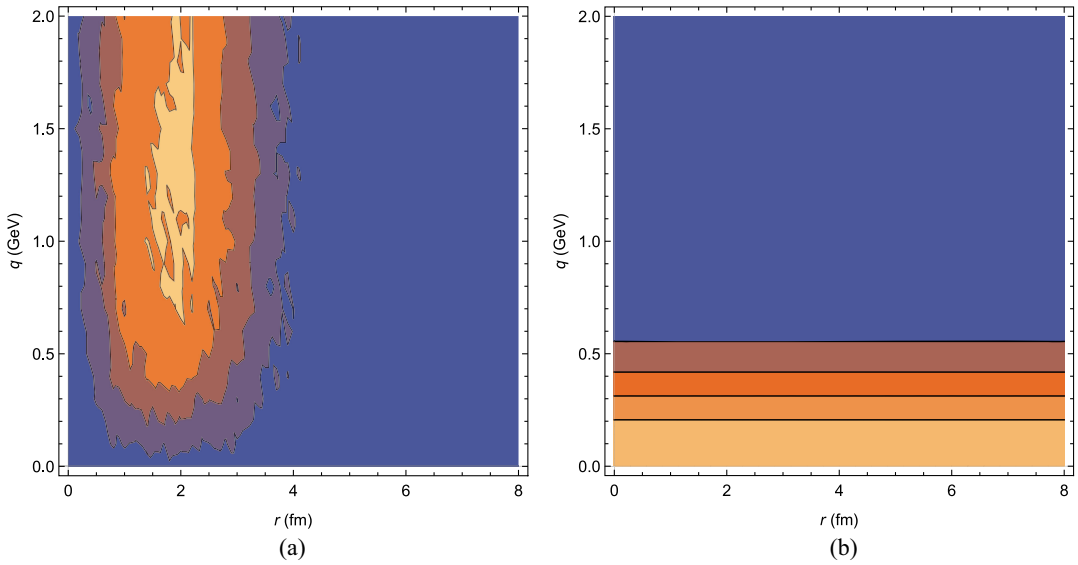

FIG. 6. Parts (a) and (b) are the Wigner densities of the source in the final state phase space of pp collisions and relativistic heavy-ion collisions, respectively.

when the size of the composite particle increases. On the other hand, in the case of heavy-ion collisions, the overlap will get larger since the distribution of the Wigner density of the source is flat. Therefore, the phase space distribution in the final state of different collisions is quite different and, therefore, affects the production yields of composite particles in a nontrivial way. This feature can be used to test the molecular picture of the many exotic hadrons discovered in recent years.

IV. SUMMARY

In this work, adopting the transport model combined with the coalescence model and using the Yukawa-type wave function, we calculated the production yields of the ΞN dibaryon for different binding energies in pp collisions. For a binding energy E_B in the range of 0.1 to 12.5 MeV, the yields are about 10^{-4}, 1 order of magnitude smaller than that of Ω, which indicates that it is possible to discover the ΞN dibaryon in LHC collisions if it indeed exists and the experimental setup is well designed.

Furthermore, the yield of ΞN can be well determined by its binding energy, a universal phenomenon. In the small E_B limit, the yield depends linearly on $\sqrt{E_B}$ and goes to zero as E_B goes to zero. The parameters in the relation encode the phase space information of constituent particles in the kinetic freeze-out stage of pp collisions. We should stress that this phenomenon is only valid for pp collisions since the phase space distributions of the final states in

different collision systems play an essential role in determining the yield.

ACKNOWLEDGMENTS

We thank Yuyan Xu for the valuable discussions. This work is partly supported by the National Natural Science Foundation of China under Grants No. 11975041 and No. 11961141004. T. W. acknowledges the support from the Chinese Scholarship Council. A. H. is partly supported by the Japanese Grant-in-Aid for Scientific Research, No. 21H04478 and No. 18H05407.

[1] K. Nakazawa *et al.*, The first evidence of a deeply bound state of $\mathrm{Xi}^- - {}^{14}\mathrm{N}$ system, Prog. Theor. Exp. Phys. **2015**, 033D02 (2015).
[2] S. Acharya *et al.*, First observation of an attractive interaction between a proton and a cascade baryon, Phys. Rev. Lett. **123**, 112002 (2019).
[3] ALICE Collaboration *et al.*, Unveiling the strong interaction among hadrons at the LHC, Nature (London) **588**, 232 (2020); **590**, E13 (2021).
[4] J. K. Ahn *et al.*, Enhanced ΛΛ production near threshold in the ${}^{12}\mathrm{C}(K^-, K^+)$ reaction, Phys. Lett. B **444**, 267 (1998).
[5] E. Friedman and A. Gal, Constraints on Ξ^- nuclear interactions from capture events in emulsion, Phys. Lett. B **820**, 136555 (2021).
[6] E. Friedman and A. Gal, Has J-PARC E07 observed a Ξ^-_{1s} nuclear state?, Phys. Lett. B **837**, 137640 (2023).
[7] T. Sakai, K. Shimizu, and K. Yazaki, H dibaryon, Prog. Theor. Phys. Suppl. **137**, 121 (2000).
[8] K. Sasaki *et al.*, ΛΛ and NΞ interactions from lattice QCD near the physical point, Nucl. Phys. **A998**, 121737 (2020).
[9] Z.-W. Liu, K.-W. Li, and L.-S. Geng, Strangeness S = −2 baryon-baryon interactions and femtoscopic correlation functions in covariant chiral effective field theory*, Chin. Phys. C **47**, 024108 (2023).
[10] E. Hiyama, K. Sasaki, T. Miyamoto, T. Doi, T. Hatsuda, Y. Yamamoto, and T. A. Rijken, Possible lightest Ξ hypernucleus with modern Ξ*N* interactions, Phys. Rev. Lett. **124**, 092501 (2020).
[11] J. Haidenbauer and U. G. Meißner, In-medium properties of a Ξ*N* interaction derived from chiral effective field theory, Eur. Phys. J. A **55**, 23 (2019).
[12] H. Garcilazo, Strangeness $-2(I, J^P) = (\frac{1}{2}, \frac{1}{2}^+)$ tribaryon resonance, Phys. Rev. C **93**, 024001 (2016).
[13] M. M. Nagels, T. A. Rijken, and Y. Yamamoto, Extended-soft-core baryon-baryon ESC08 model III. $S = -2$ hyperon-hyperon/nucleon interactions, Phys. Rev. C **102**, 054003 (2020).
[14] K. Aamodt *et al.*, Strange particle production in proton-proton collisions at $\sqrt{s} = 0.9$ TeV with ALICE at the LHC, Eur. Phys. J. C **71**, 1594 (2011).
[15] B. Abelev *et al.*, Multi-strange baryon production in pp collisions at $\sqrt{s} = 7$ TeV with ALICE, Phys. Lett. B **712**, 309 (2012).
[16] J. Adam *et al.*, Measurement of pion, kaon and proton production in proton-proton collisions at $\sqrt{s} = 7$ TeV, Eur. Phys. J. C **75**, 226 (2015).
[17] B.-H. Sa, D.-M. Zhou, Y.-L. Yan, X.-M. Li, S.-Q. Feng, B.-G. Dong, and X. Cai, PACIAE 2.0: An updated parton and hadron cascade model (program) for the relativistic nuclear collisions, Comput. Phys. Commun. **183**, 333 (2012).
[18] J. L. Nagle, B. S. Kumar, D. Kusnezov, H. Sorge, and R. Mattiello, Coalescence of deuterons in relativistic heavy ion collisions, Phys. Rev. C **53**, 367 (1996).
[19] S. Sombun, K. Tomuang, A. Limphirat, P. Hillmann, C. Herold, J. Steinheimer, Y. Yan, and M. Bleicher, Deuteron production from phase-space coalescence in the UrQMD approach, Phys. Rev. C **99**, 014901 (2019).
[20] M. Gyulassy, K. Frankel, and E. a. Remler, Deuteron formation in nuclear collisions, Nucl. Phys. **A402**, 596 (1983).
[21] S. Cho *et al.*, Identifying multiquark hadrons from heavy ion collisions, Phys. Rev. Lett. **106**, 212001 (2011).
[22] L. W. Chen, V. Greco, C. M. Ko, S. H. Lee, and W. Liu, Pentaquark baryon production at the relativistic heavy ion collider, Phys. Lett. B **601**, 34 (2004).
[23] S. Zhang and Y.-G. Ma, Ω-dibaryon production with hadron interaction potential from the lattice QCD in relativistic heavy-ion collisions, Phys. Lett. B **811**, 135867 (2020).
[24] L. Zhang, S. Zhang, and Y.-G. Ma, Production of Ω*NN* and ΩΩ*N* in ultra-relativistic heavy-ion collisions, Eur. Phys. J. C **82**, 416 (2022).
[25] V. Greco, C. M. Ko, and P. Levai, Parton coalescence at RHIC, Phys. Rev. C **68**, 034904 (2003).
[26] V. Greco, C. M. Ko, and P. Levai, Parton coalescence and anti-proton/pion anomaly at RHIC, Phys. Rev. Lett. **90**, 202302 (2003).
[27] T. Sjostrand, S. Mrenna, and P. Z. Skands, PYTHIA 6.4 physics and manual, J. High Energy Phys. 05 (2006) 026.
[28] R. Mattiello, H. Sorge, H. Stoecker, and W. Greiner, Nuclear clusters as a probe for expansion flow in heavy ion reactions at 10-A/GeV–15-A/GeV, Phys. Rev. C **55**, 1443 (1997).
[29] A. Hosaka, T. Iijima, K. Miyabayashi, Y. Sakai, and S. Yasui, Exotic hadrons with heavy flavors: X, Y, Z, and related states, Prog. Theor. Exp. Phys. **2016**, 062C01 (2016).

[30] S. H. Kim, Y. Ichikawa, S. Hayakawa, and J. K. Ahn, Search for the H-dibaryon near $\Lambda\Lambda$ and $\Xi^- p$ thresholds via $^{12}\mathrm{C}(K^-, K^+)$ reactions at J-PARC, J. Phys. Soc. Jpn. Conf. Proc. **37**, 021002 (2022).

[31] F.-K. Guo, C. Hanhart, U.-G. Meißner, Q. Wang, Q. Zhao, and B.-S. Zou, Hadronic molecules, Rev. Mod. Phys. **90**, 015004 (2018); **94**, 029901(E) (2022).

[32] E. Braaten, M. Kusunoki, and S. Nussinov, Production of the X(3872) in B meson decay by the coalescence of charm mesons, Phys. Rev. Lett. **93**, 162001 (2004).

[33] P. Artoisenet and E. Braaten, Production of the X(3872) at the tevatron and the LHC, Phys. Rev. D **81**, 114018 (2010).

[34] S. Cho *et al.*, Exotic hadrons in heavy ion collisions, Phys. Rev. C **84**, 064910 (2011).